# Supplementary material for "Increased Late Pleistocene erosion rates during fluvial aggradation in the Garhwal Himalaya, northern India"

Dirk Scherler[a,b,c,*], Bodo Bookhagen[d,e], Hendrik Wulf[f], Frank Preusser[g], Manfred R. Strecker[e],

[a] Division of Geological and Planetary Sciences, California Institute of Technology, Pasadena, USA

[b] Earth Surface Geochemistry, Helmholtz Centre Potsdam GFZ German Research Centre for Geosciences, Potsdam, Germany

[c] Institute of Geological Sciences, Free University of Berlin, Berlin, Germany

[d] Department of Geography, University of California, Santa Barbara, USA

[e] Institute of Earth and Environmental Science, University Potsdam, Potsdam, Germany

[f] Department of Geography, University of Zurich, Zurich, Switzerland

[g] Institute of Earth and Environmental Sciences - Geology, University of Freiburg, Freiburg, Germany

[*] Corresponding author: e-mail: scherler@gfz-potsdam.de; phone: +49 331 288-28646

## 1 Dating procedures – OSL lab Bern

Three samples (DS6-16, DS6-92, DS6-95) were taken in opaque containers and opened under subdued red-light laboratory illumination. The outer part of the sampled material was removed as it may have been exposed to light but was used for determination of dose rate relevant elements using high-resolution low-level gamma spectrometry (VKTA Rossendorf e.V., Germany). The remaining material was first dried, subsequently sieved and chemically pre-treated using HCl, $H_2O_2$ and Na-oxalate. A K-feldspar and quartz fraction were isolated using heavy liquid separation ($\rho$ = 2.58 and 2.70 g $cm^{-3}$). The quartz fraction was etched in 40 % HF for 60 min to remove remaining feldspar and the outer rim of the grains. IR test revealed that the samples were still contaminated by feldspar but this contamination was successfully removed by an additional etching step in $H_2SiF_6$ for one week.

All measurements were carried out on a Risø TL/OSL DA-20 reader, equipped with IR and blues diode light sources. All measurements for Optically Stimulated Luminescence (OSL) on quartz and InfraRed Stimulated Luminescence (IRSL) on K-feldspars were carried out on small (2 mm) aliquots, a procedure that has been successfully applied for dating of poorly bleached sediments (Preusser et al., 2007). Each aliquot of quartz was first checked for any feldspar contamination and then measured using the single aliquot regenerative dose protocol of Murray and Wintle (2000), with preheating at 230°C for 10 s prior to all OSL measurements. These measurements revealed poor OSL characteristics of the investigated quartz, namely relatively low OSL intensities and the absence of fast components in the OSL signal (Fig. S1). Such signal characteristics have repeatedly observed for samples from the foreland of young orogenic systems and have resulted in significant underestimation of quartz OSL ages (e.g., Steffen et al., 2009a). Previous experience has shown that under such circumstances using K-feldspars is more promising (Steffen et al., 2009b), which led us to use this natural dosimeter.

IRSL measurements were carried out using the modified SAR protocol of Preusser (2003). Firstly, dose recovery tests have been carried out to investigate the influence of preheating on Equivalent Dose (De) determination (Fig. S2). This showed some overestimation of De for preheat at 270°C and 290°C, followed by a significant drop for preheating at 310°C. The overestimation is likely caused by thermal transfer (Rhodes and Bailey, 1997). As a consequence, preheating at 250°C for 10 s was carried out for De determination.

The K-feldspar show perfectly behaving IRSL signals and all samples are in the exponentially increasing part of the dose response curve (Fig. S3). For each of the sample, 12 aliquots have been measured, revealing nicely Gaussian shaped dose distributions (Fig. S4). This is interpreted to reflect completely bleaching of IRSL prior to deposition. As recent publications have questioned the reliability of storage tests to quantify potential loss of the IRSL (Gaar and Preusser, 2012; Lowick et al., 2012), no such test have been conducted. As a consequence, and in the apparent absence of partial bleaching, the IRSL ages have to be considered as minimum estimates, as fading could lead to age underestimation. Calculation of ages was carried out using ADELE software. The calculated contribution from cosmic radiation after Prescott and Hutton (1994) was taken into account with a relative uncertainty of 10%. Potassium content of feldspar was assumed to be 12.5 ± 1.0 % following the estimates of Huntley and Baril (1997).

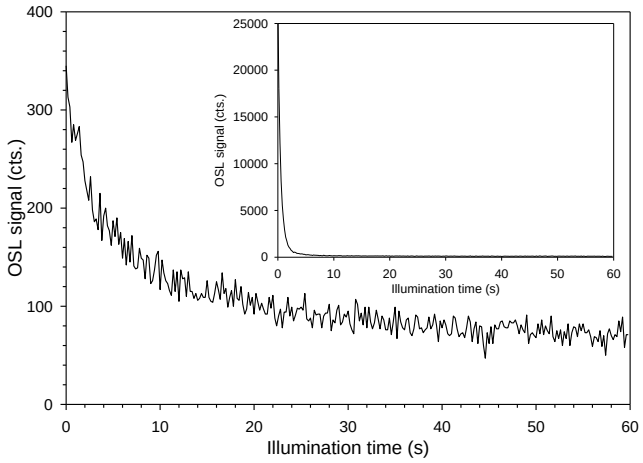


Figure S1: Typically OSL decay curve for one of the Himalayan samples compared to a nicely behaving quartz from the Bolivian lowlands (inset) that show a bright and fast components dominated signal.

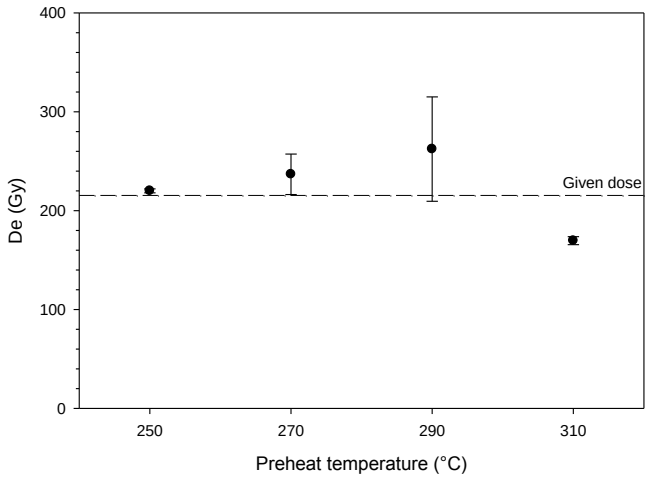

Figure S2: Dose recovery test reveals overestimation of given dose for preheat temperatures of 270/290°C.

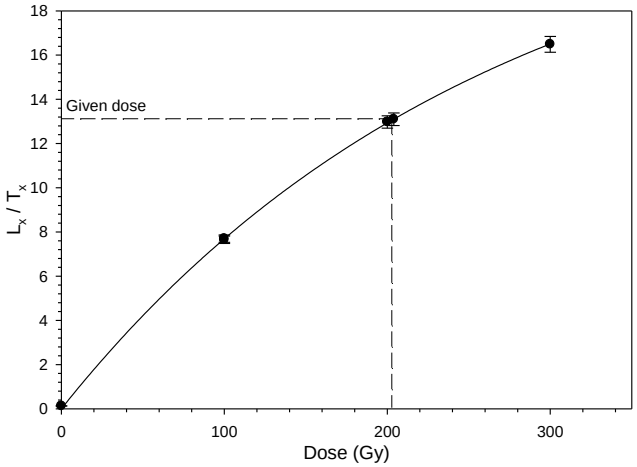


Figure S3: Typical IRSL dose response curve of K-feldspars.

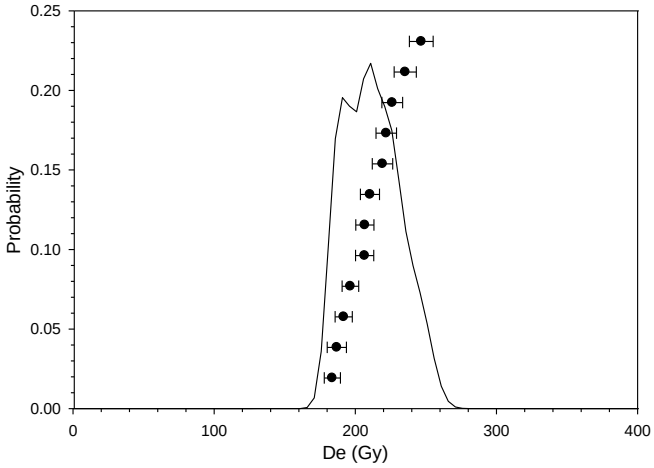


Figure S4: Dose distribution plot of sample DS6-16 shows a Gaussian distribution interpreted to indicate complete bleaching of the IRSL signal at deposition.

## 2 Valley floor reconstruction

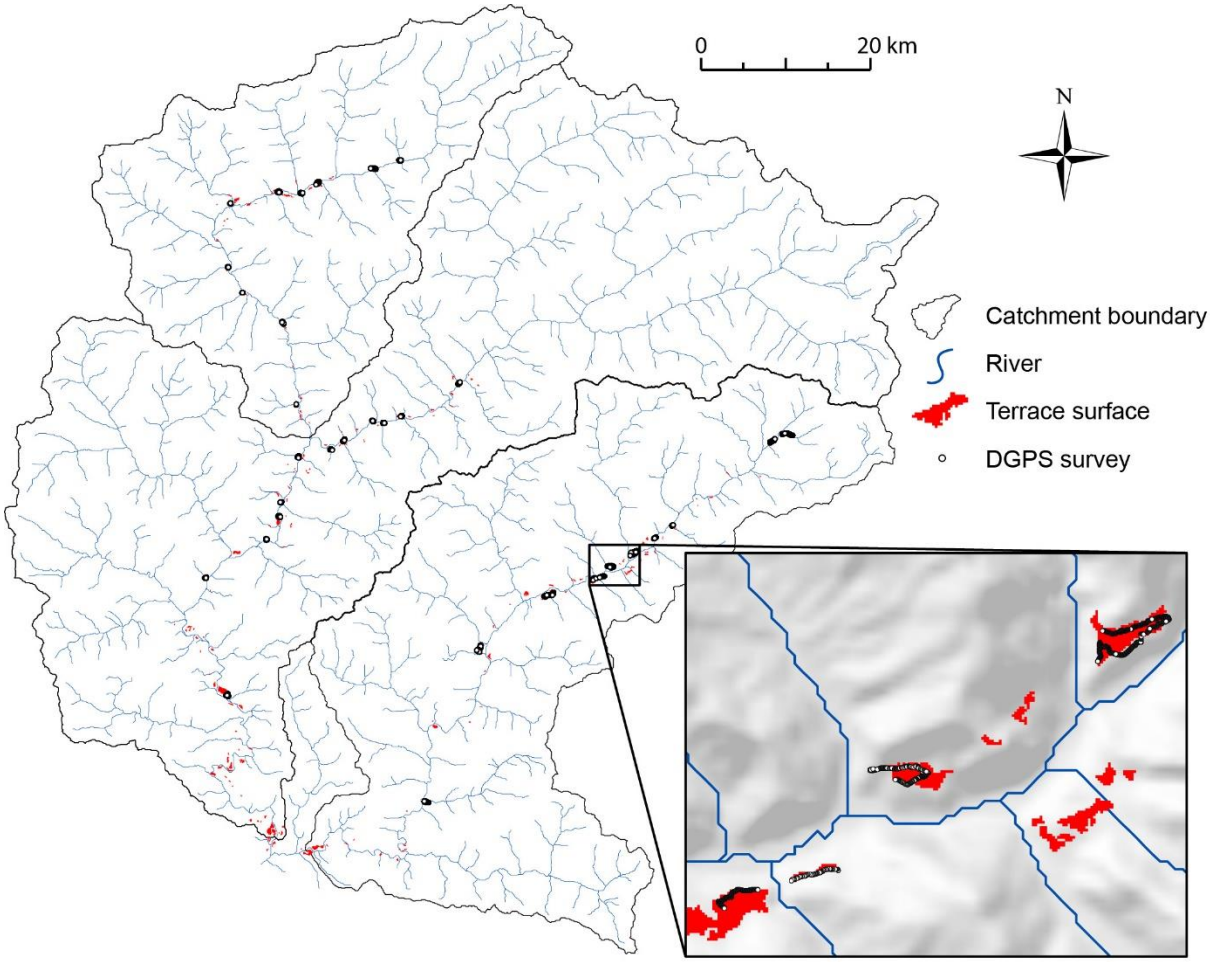


Figure S5: Map of the Yamuna catchment showing the drainage network and the terrace surfaces mapped with satellite imagery (red) and by differential GPS (DGPS) in the field (points). Subset in lower right corner shows exemplary terrace details not visible in large scale map.

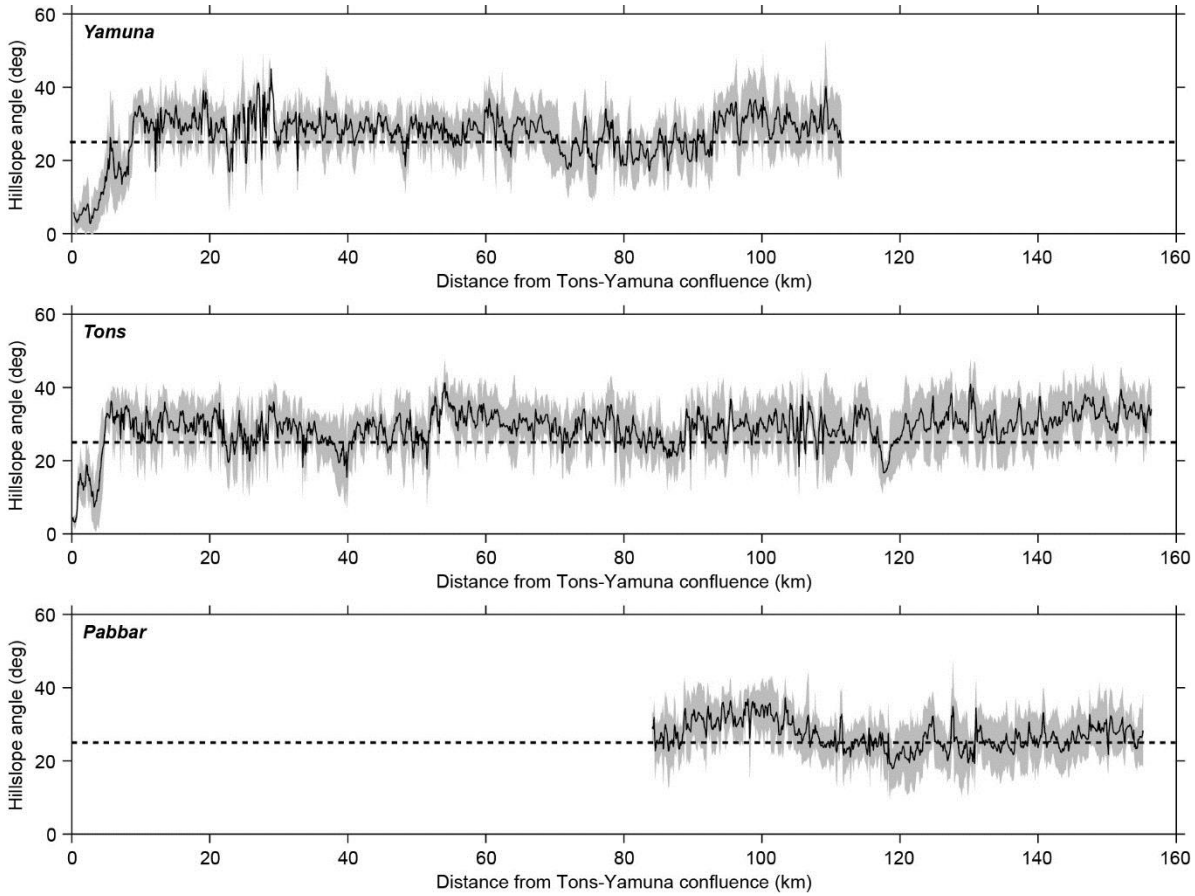


Figure S6: To reconstruct the subsurface geometry of the valley floor along the three trunk river valleys, we measured the hillslope angles above the prominent valley fill and within a swath of 5 km width that is centered on a smooth plan-view trace of the rivers. The above panels show the mean (black solid line) hillslope angles with one standard deviation (gray polygon). Although the average angle is often close to 30°, we used 25° (black dashed line) as our reference value for reconstructing the valley floor by projecting the hillslopes into the subsurface. The resulting surface elevations were taken as the minimum of the projected and the actual present-day surface elevations.

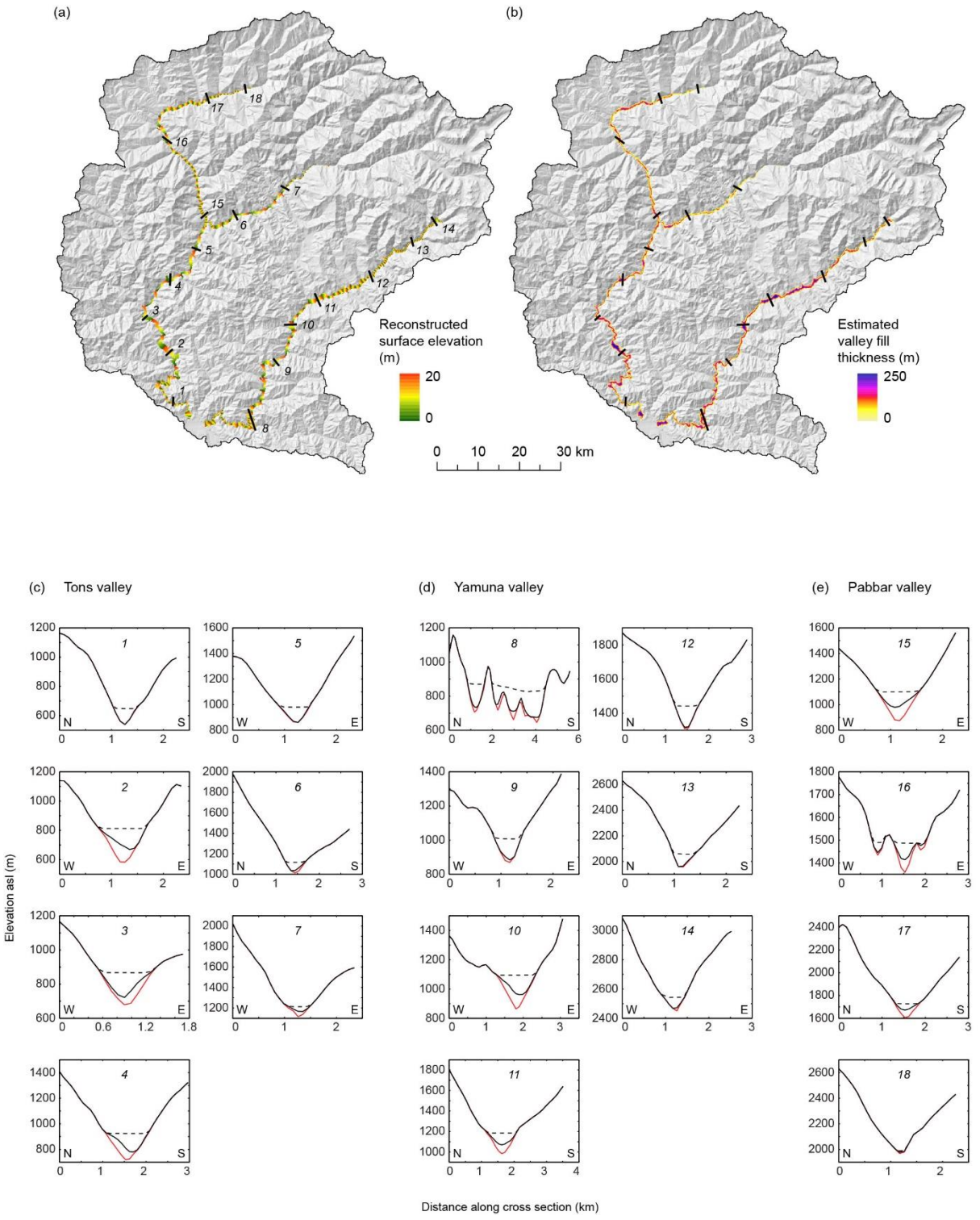


Figure S7: Geometry of the reconstructed valley fill. (a) Surface elevation of the valley fill at the end of the aggradation and before re-incision. The colors cycle through 20-m contour intervals. Black lines indicate topographic profiles shown in (c). (b) Reconstructed thickness of the valley fill. (c) Topographic profiles transverse to the orientation of the valley and showing the modern topography (black solid line), the reconstructed surface of the valley fill at the end of the aggradation period (black dashed line), and the reconstructed floor of the valley prior to the aggradation (red line).

## 3 Sample information

### 3.1 Yamuna Valley

In the Yamuna Valley, we collected our samples mainly from two locations. One (Y2) is located near the village of Lakha Mandal. Figure S8 provides an overview of this area along with a field photograph and sketch of one of the outcrops. In total, we collected 7 different samples near this location. Three more samples (DS7-53A, DS7-54A&B) were collected near the village of Tatou (Y1), where the exposed terrace nicely documents one fill sequence.

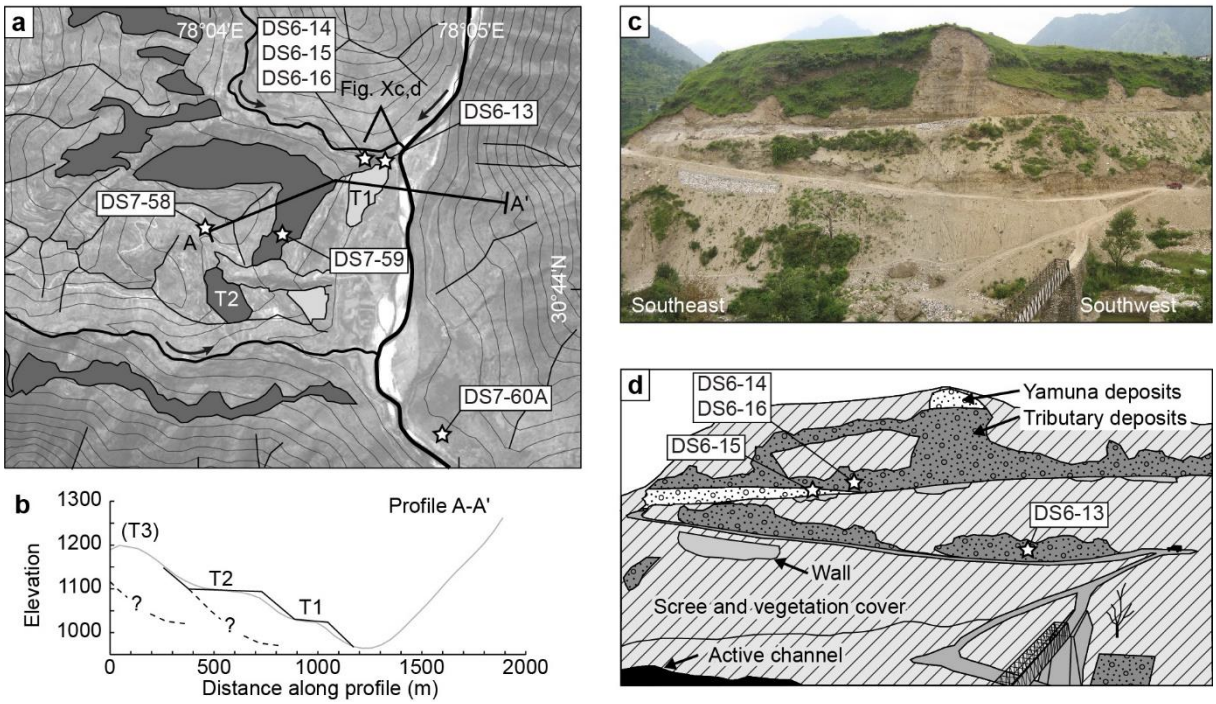


Figure S8: Overview of sampling locations near Lakha Mandal (Y2). (a) Map-view of sampling locations. Contour lines spaced 50 m. 'T2' marks the pronounced top surface of the main valley fill. 'T1' marks a terrace surface cut during the incision of the T2 valley fill. Stars show sample locations. (b) Topographic profile showing relationship between old (T3) and young (T1, T2) terrace surfaces. (c) Field photograph of fill terrace T1 where several samples were taken. (d) Sketch of photograph shown in c, with sampling locations indicated.

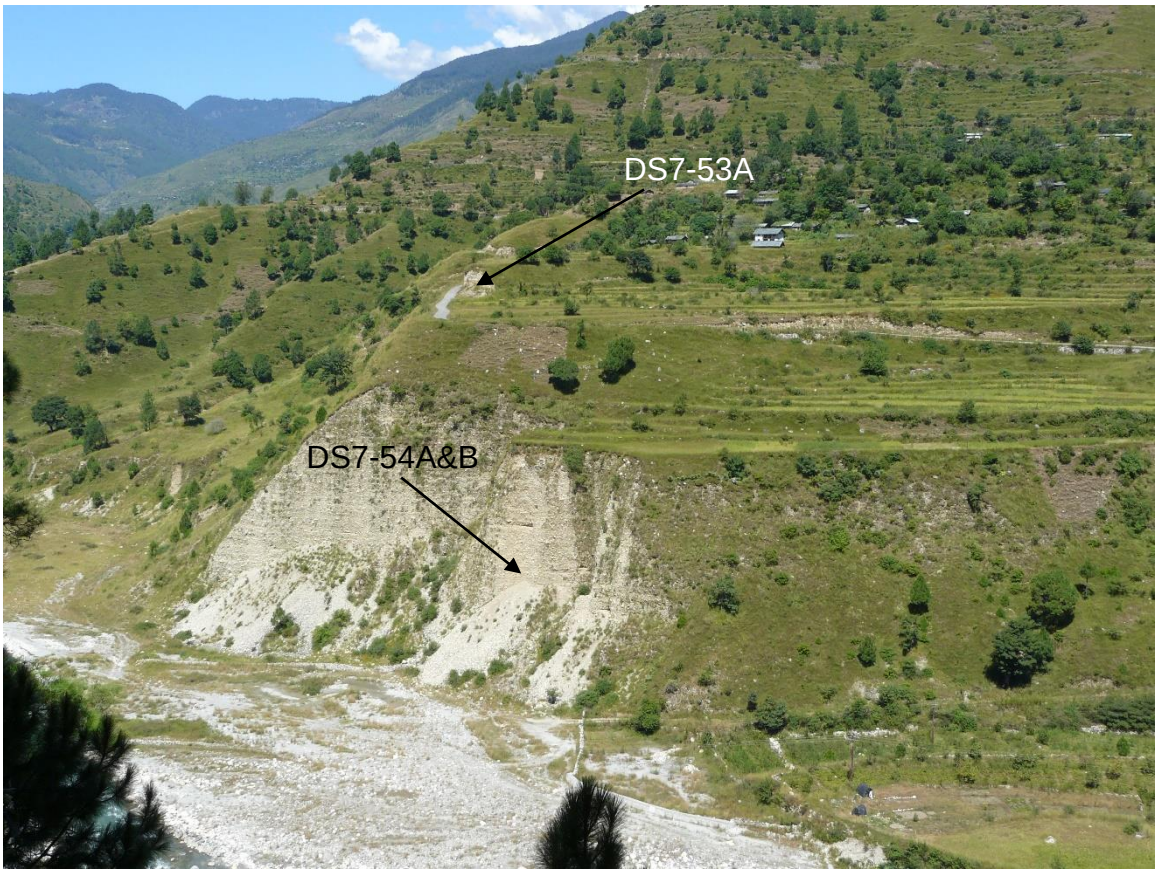


Figure S9: Overview of sampling location near the village of Tatou. Sample DS7-53A is stratigraphically younger than DS7-54A&B. Samples DS7-54A&B were collected close to the present-day river.

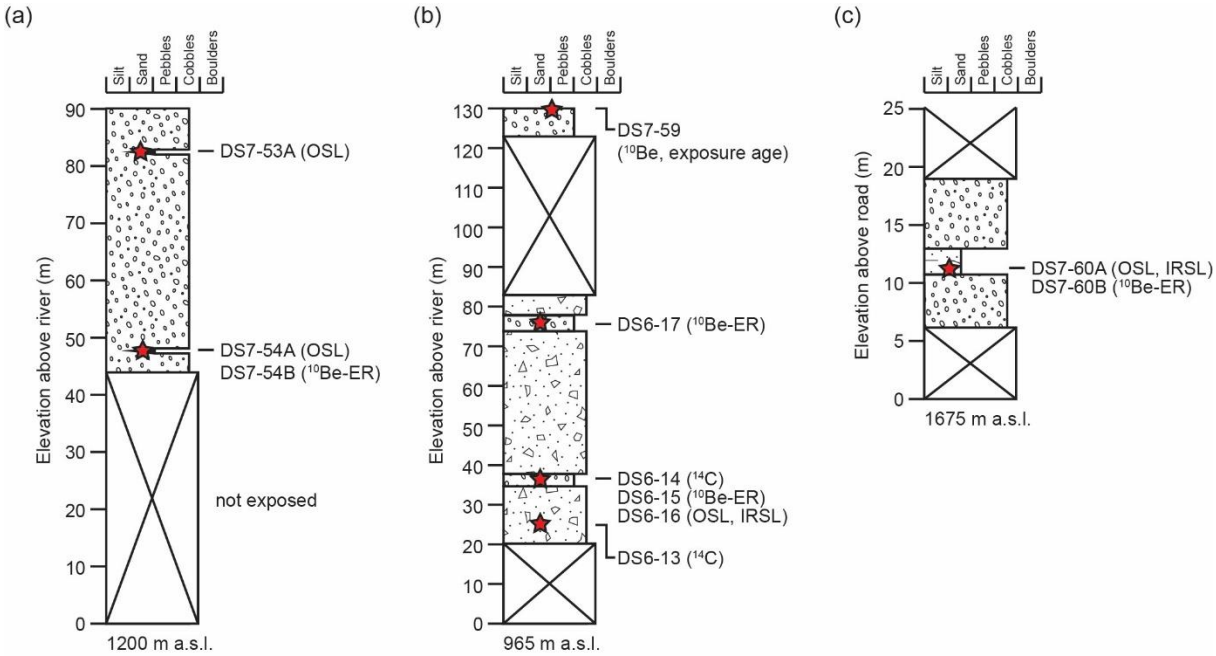

Figure S10: Graphic sedimentary logs from the sampled outcrops in the Yamuna Valley (a) near the village Tatou, (b, c) near the village Lakha Mandal. $^{10}$Be-ER indicates sand sample for $^{10}$Be-derived paleo-erosion rates.

### 3.1.1 Y2: DS6-13 ($^{14}$C)

Figure S11: Outcrop of tributary deposits near Lakha Mandal.

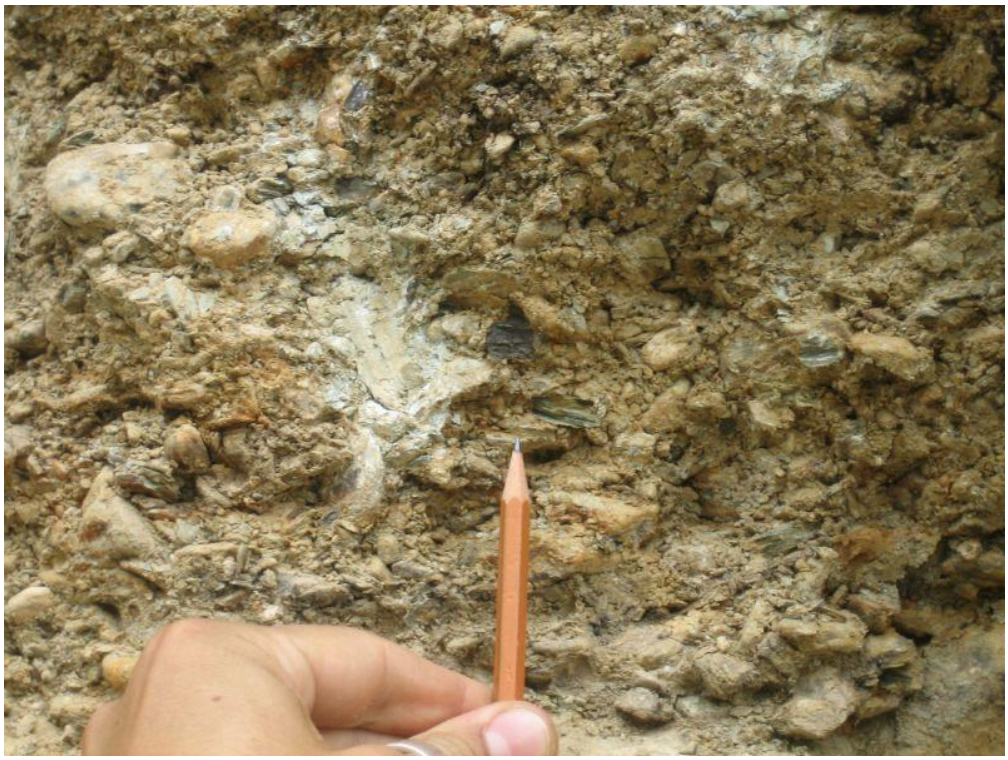

Figure S12: Close-up of charcoal piece sampled for $^{14}C$ dating.

### 3.1.2 Y2: DS6-14 ($^{14}C$)

Figure S13: Outcrop of tributary deposits on top of light-colored deposits of the Yamuna River near Lakha Mandal.

Figure S14: Close-up of charcoal pieces contained in fine-grained deposits, which were sampled for $^{14}C$ dating.

### 3.1.3 Y2: DS6-15 ($^{10}$Be, paleo-erosion rate)

Figure S15: Outcrop showing cobble-dominated, light-colored Yamuna deposits with a sand lens from which a sample for $^{10}$Be-derived paleo-erosion rates was collected.

### 3.1.4 Y2: DS6-16 (OSL, IRSL)

Figure S16: Luminescence sample location after recovery of steel-tube. Below sampling point are light-colored Yamuna deposits, above sampling point are dark-colored tributary deposits.

### 3.1.5 Y2: DS6-17 ($^{10}$Be, paleo-erosion rate)

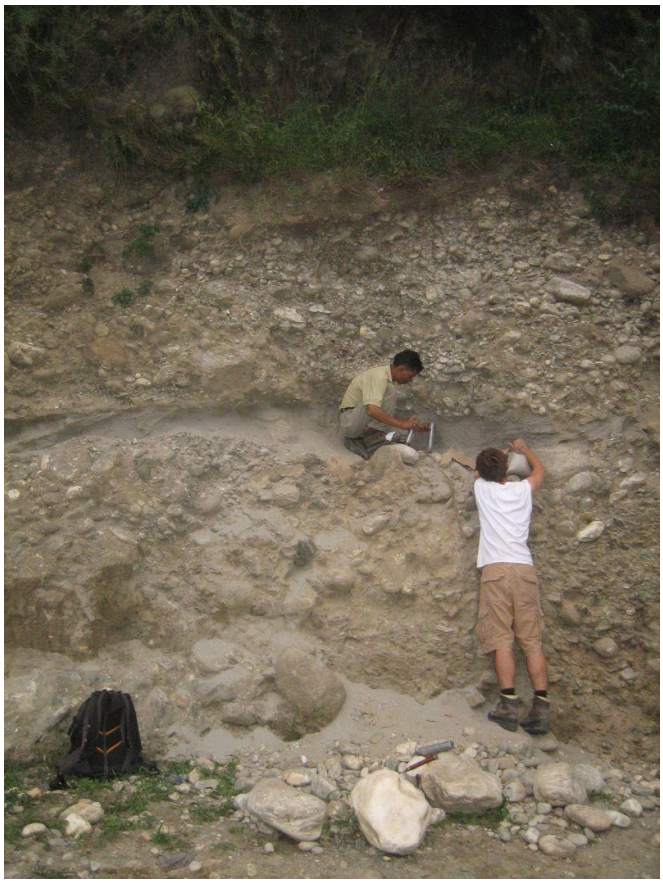

Figure S17: Sand sample for paleo-erosion rates was sampled from sand lens that was imbedded in light-colored Yamuna deposits. We attempted to collect a tube sample (see photo) for dating the deposits, but aborted the plan due to unsafe conditions during hammering the tube into the deposits.

### 3.1.6 Y2: DS7-58 (OSL)

Figure S18: Outcrop exposed at road cut where sample was collected.

Figure S19: Close-up of ~20 cm thick medium-sand lens where sample was taken from.

### 3.1.7 Y2: DS7-59 ($^{10}$Be exposure age)

Figure S20: Agriculturally used terrace surface, from which pebbles were collected for surface exposure dating.

Figure S21: View of ground surface from which >30 well-rounded pebbles were collected for surface exposure dating.

### 3.1.8 Y2: DS7-60A (OSL) & DS7-60B ($^{10}$Be paleo-erosion rate)

Figure S22: Terrace deposits exposed near road where sample has been collected (person for scale).

Figure S23: Sample was collected from near the base of a ~2-m thick sand lens in between coarser deposits.

Figure S24: Close-up of fine-sand deposits where tube sample was taken from. Paleo-erosion rate sample was taken from the same location.

### 3.1.1 Y1: DS7-53A (OSL)

Figure S25: Terrace outcrop at road cut, which exposes pebble-to-boulder sized well-rounded fluvial deposits.

Figure S26: Coarse-sand lens (25 cm thick) where sample was taken from. See hammer on the left for scale and tube on the right for sampling location.

Figure S27: Close up of sample location with inserted tube, before recovery.

### 3.1.1 Y1: DS7-54A (OSL) & DS7-54B ($^{10}$Be, paleo-erosion rate)

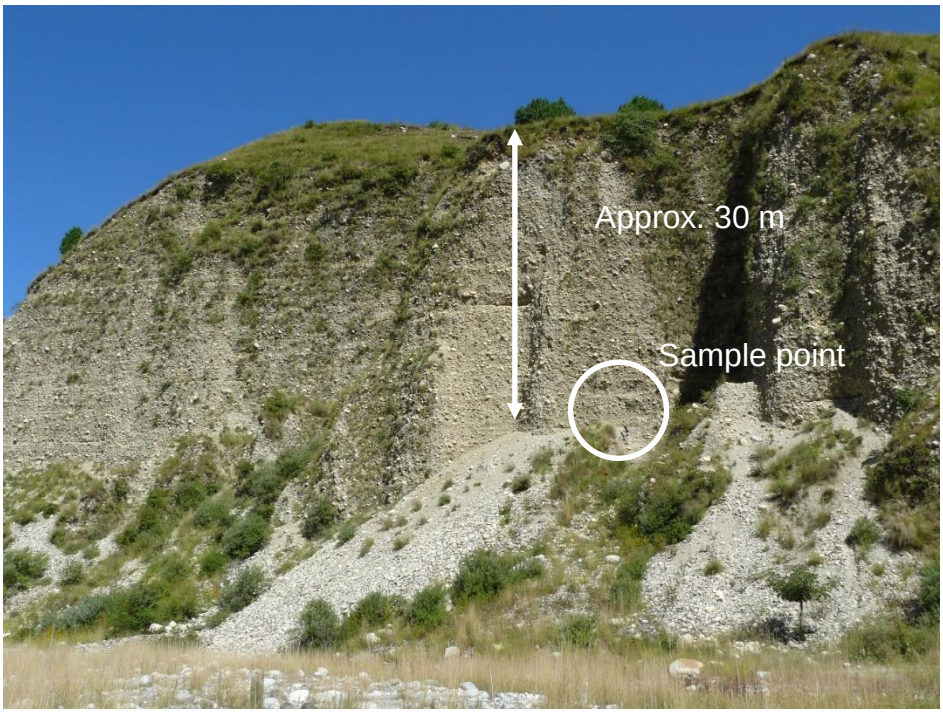


Figure S28: Section exposed near present-day river.

Figure S29: Sand lens where the samples were taken from.

Figure S30: Close up of sample location within coarse-sand lens of ~18 cm thickness with hammer for scale.

### 3.2 Pabbar

In the Pabbar Valley, we collected four samples from locations that are in close proximity to each other. Part of the samples were taken from sediments that were deposited by the Pabbar River while others were taken from deposits that are related to tributary rivers. Nevertheless.

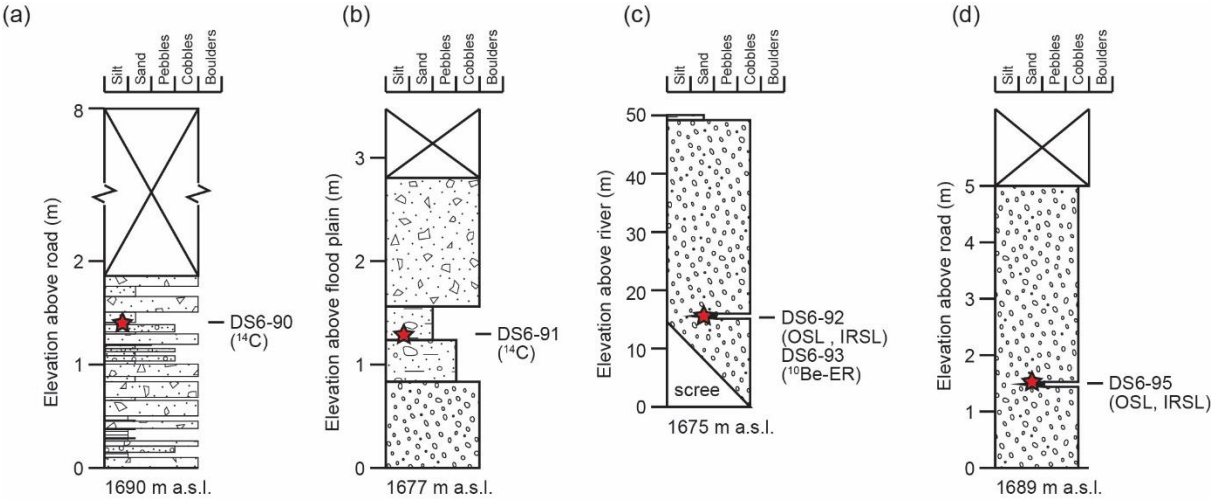


Figure S31: Graphic sedimentary logs from the sampled outcrops in the Pabbar Valley near the village Badyara.

### 3.2.1 P1: DS6-90 ($^{14}$C)

Figure S32: Sandy tributary deposits with layering inclined to the left (east).

Figure S33: Close-up of sandy deposits with interspersed charcoal pieces.

### 3.2.2 P1: DS6-91 ($^{14}$C)

Figure S34: Close-up of sample location near present-day river bed. Dark layers near the center of the photograph contains charcoal pieces, which have been sampled.

### 3.2.3 P1: DS6-92 (OSL, IRSL) & DS6-93 ($^{10}$Be, paleo-erosion rate)

Figure S35: Terrace outcrop (~50 m high), with its base near the present-day river level. Note person for scale.

Figure S36: Close-up of terrace outcrop and sampling tube within coarse-sand layer. Sand sample for paleo-erosion rates was sampled from the same layer.

### 3.2.4 P1: DS6-95 (OSL, IRSL)

Figure S37: Terrace deposit outcrop with sandy lens (in the middle of the picture), from where a tube sample was taken.

Figure S38: Close-up of sand lens with tube sample.

### 3.3 Tons Valley

In the Tons Valley, we collected our samples from three different locations. ‘T0’ is highest upstream and ‘T2’ is farthest downstream.

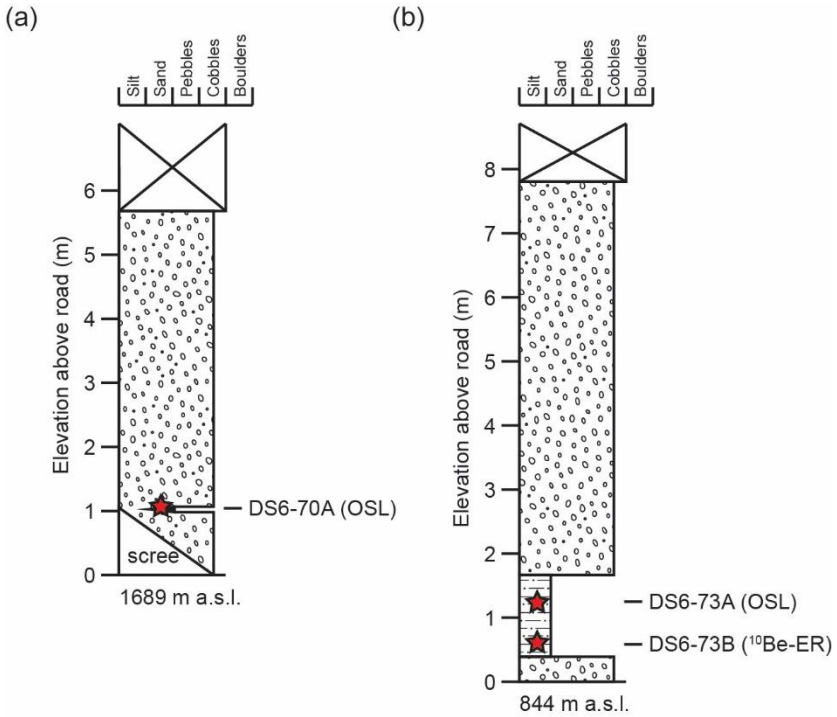


Figure S39: Graphic sedimentary logs from the sampled outcrops in the Tons Valley (a) near the village Tuini, (b) near the village Dharwa.

### 3.3.1 T0: DS7-65 ($^{10}$Be, exposure dating)

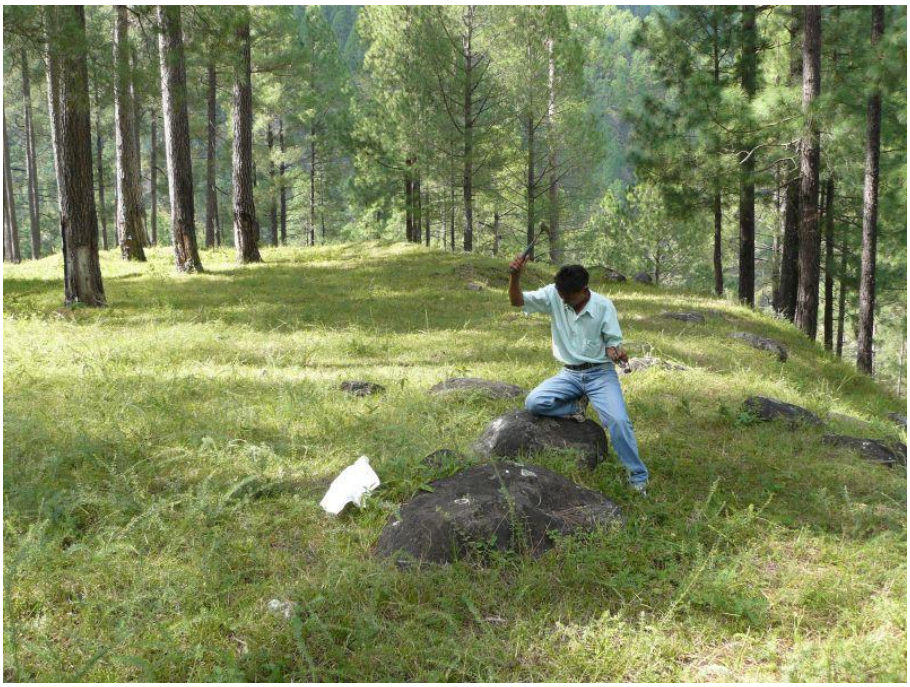

Figure S40: Terrace surface with boulders that we sampled for surface exposure dating. We amalgamated rock chips from 12 boulders similar in size to the one shown on the photograph.

### 3.3.2 T1: DS7-70A (OSL)

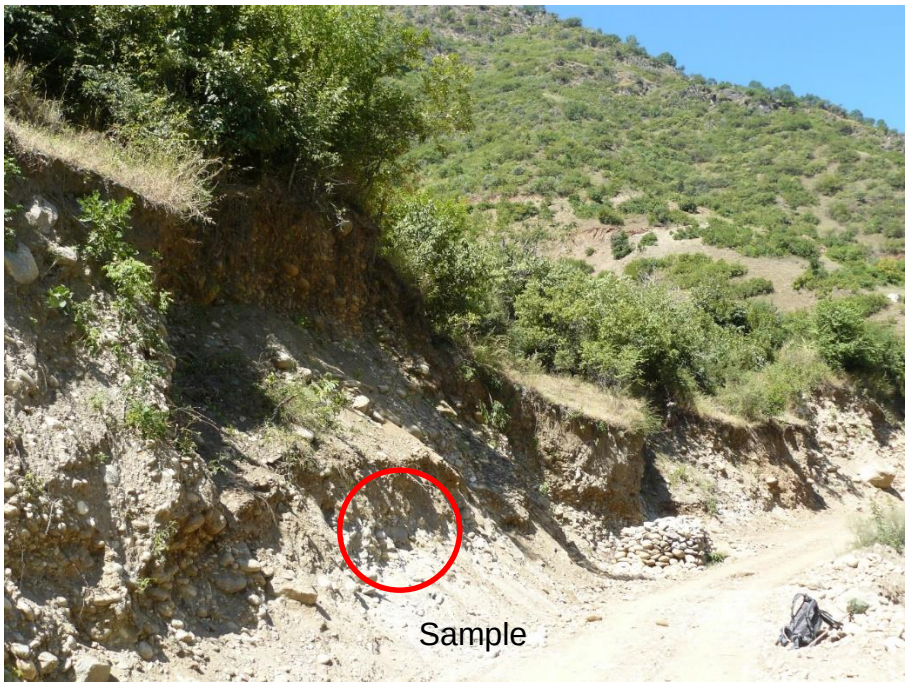


Figure S41: Section exposed at road cut where sample has been collected (see bag to the right for scale).

Figure S42: Sample was collected from a coarse-sand lens (15 cm thick) near the ground surface (see hammer for scale).

Figure S43: Close-up of tube insertion into sand lens.

### 3.3.3 T2: DS7-73A (OSL) & DS7-73C ($^{10}$Be, paleo-erosion rate)

Figure S44: Outcrop exposed at road cut.

Figure S45: OSL-sample was collected near the base of a ~1.5-m thick sand-to-silt lens close to the ground surface. Paleo-erosion rate sample was collected from the base of this layer, where grain sizes were dominated by sand.

Figure S46: Close-up of sampling point where tube has been inserted.

### 3.3.4 T1: DS7-80 ($^{10}$Be, paleo-erosion rate)

Figure S47: Terrace outcrop of Tons deposits. Sand sample for paleo-erosion rates was collected from sand layer near road.

## 4 References


Gaar, D., Preusser, F., 2012. Luminescence dating of mammoth remains from northern Switzerland. *Quaternary Geochronology* 10, 257-263.

Huntley, D.J., Baril, M.R., 1997. The K content of the K-feldspars beeing measured in optical dating or in thermoluminescence dating. *Ancient TL* 15, 11-14.

Lowick, S. E., Trauerstein, M., Preusser, F., 2012. Testing the application of post IR-IRSL dating to fine grain waterlain sediments. *Quaternary Geochronology* 8, 33-40.

Murray, A.S., Wintle, A.G., 2000. Luminescence dating of quartz using an improved single-aliquot regenerative-dose protocol. *Radiation Measurements* 33, 57-73.

Prescott, J.R., Hutton, J.T., 1994. Cosmic ray contributions to dose rates for luminescence and ESR dating: Large depths and long-term time variations. *Radiation Measurements* 23, 497-500.

Preusser, F., 2003. IRSL dating of K-rich feldspars using the SAR protocol: Comparison with independent age control. *Ancient TL* 21, 17-23.

Preusser, F., Blei, A., Graf, H., Schlüchter, C., 2007. Luminescence dating of Würmian (Weichselian) proglacial sediments from Switzerland: methodological aspects and stratigraphical conclusions. *Boreas* 36, 130-142.

Rhodes, E.J., Bailey, R.M., 1997. The effect of thermal transfer on the zeroing of quartz from recent glaciofluvial sediments. *Quaternary Science Reviews* (Quaternary Geochronology) 16, 291-298.

Steffen, D., Preusser, F., Schlunegger, F. 2009. OSL quartz age underestimation due to unstable signal components. *Quaternary Geochronology* 4, 353-362.

Steffen, D., Schlunegger, F., Preusser, F. 2009. Drainage basin response to climate change in the Pisco Valley, Peru. *Geology* 37, 491-494